Journal of Alzheimer's Disease 14 (2008) 235–245
IOS Press

Three-Dimensional Tomographic Imaging and Characterization of Iron Compounds within Alzheimer's Plaque Core Material

Joanna F. Collingwood[a], Ryan K. K. Chong[b], Takeshi Kasama[b,c], Lionel Cervera-Gontard[b], Rafal E. Dunin-Borkowski[b,c,d], George Perry[e,f], Mihály Pósfai[g], Sandra L. Siedlak[e], Edward T. Simpson[b], Mark A. Smith[e] and Jon Dobson[a,*]

[a]*Institute of Science and Technology in Medicine, Keele University, Thornburrow Drive, Hartshill, Stoke-on-Trent, ST4 7QB, UK*

[b]*Department of Materials Science and Metallurgy, University of Cambridge, Pembroke Street, Cambridge, CB2, 3QZ, UK*

[c]*Frontier Research System, The Institute of Physical and Chemical Research, Hatoyama, Saitama 350-0395, Japan*

[d]*Center for Electron Nanoscopy, Technical University of Denmark, DK-2800 Kongens Lyngby, Denmark*

[e]*Department of Pathology, Case Western Reserve University, Cleveland Ohio, USA*

[f]*College of Sciences, University of Texas at San Antonio, San Antonio, Texas, USA*

[g]*Department of Earth and Environmental Sciences, University of Veszprém, POB 158, H-8201, Hungary*

Handling editor: Ralph Martins

Abstract. Although it has been known for over 50 years that abnormal concentrations of iron are associated with virtually all neurodegenerative diseases, including Alzheimer's disease, its origin, nature and role have remained a mystery. Here, we use high-resolution transmission electron microscopy (HR-TEM), energy dispersive X-ray (EDX) spectroscopy and electron energy-loss spectroscopy (EELS), electron tomography, and electron diffraction to image and characterize iron-rich plaque core material – a hallmark of Alzheimer's disease pathology – in three dimensions. In these cores, we unequivocally identify biogenic magnetite and/or maghemite as the dominant iron compound. Our results provide an indication that abnormal iron biomineralization processes are likely occurring within the plaque or the surrounding diseased tissue and may play a role in aberrant peptide aggregation. The size distribution of the magnetite cores implies formation from a ferritin precursor, implicating a malfunction of the primary iron storage protein in the brain.

Keywords: Alzheimer's disease, amyloid, electron microscopy, ferritin, imaging, iron, magnetite, senile plaque core, tomography

INTRODUCTION

Iron plays an essential physiological role in virtually all organisms. The ability of iron to change its valence state enables it to participate in energetic processes and, in animals, it binds and transports molecular oxygen via hemoglobin. In the human brain, iron is necessary for both neurotransmitter synthesis and myelination and, as in the rest of the body, is stored in a ferrihydrite-like structure within the ferritin protein. However, in spite of these important roles, iron can also be toxic, with certain forms participating in the production of free radicals. In recent years, anomalous accumulations of iron have been shown to be associated with a wide variety of neurodegenerative disorders, including

*Corresponding author: Jon Dobson, Institute for Science and Technology in Medicine, Keele University, Stoke-on-Trent, ST4 7QB, United Kingdom. Tel.: +44 1782 554 253; Fax: +44 1782 717 079; E-mail: bea22@keele.ac.uk.

ISSN 1387-2877/08/$17.00

Alzheimer's disease (AD), Parkinson's and Huntington's diseases, progressive supranuclear palsy (PSP), and rarer diseases such as amyotrophic lateral sclerosis, Friedreich's ataxia, neuroferritinopathy and others [5, 9,11,33,58]. This association with AD was reported as early as 1953 [22], however, in the more than 50 years since this study was performed, progress towards identifying specific iron compounds, their origin and their potential role in neurodegeneration, has been slow.

In humans, non-heme brain iron tends to accumulate until the age of 40, with further region-specific increases in brain iron in later life [12,23,58,59]. Iron is implicated in the pathogenesis of AD, as it is associated with oxidative stress and neurotoxicity, and there is evidence that the accumulation of iron and oxidative stress precede the formation of senile plaques and neurofibrillary tangles [6,7,39]. Iron is unusual in that it adopts both the ferric (Fe^{3+}) and ferrous (Fe^{2+}) valence states *in vivo*, and utilizes this property in uptake, transport, and storage. An excess of ferrous iron can be toxic, leading to subsequent death of neurons by apoptosis. For instance, ferrous iron reacting with hydrogen peroxide (H_2O_2) via the Fenton reaction, or with peroxynitrates, catalyzes oxidant-mediated damage [7,21].

At present, the role of iron and other metals in neurodegenerative disease is not well understood. However, evidence is mounting that synergistic mechanisms are likely to exist between iron and amyloid-β ($A\beta_{42}$) – the principal component of senile plaques in AD – and other disease-related proteins [5,26,34,39,50,58]. Iron has been shown to promote $A\beta_{42}$ aggregation and toxicity *in vitro* [50] and to set up redox cycles that are not only $A\beta_{42}$-dependent but result in the stabilization of a ferric/ferrous iron mixture and the production of particle and peptide aggregates [34]. There is also evidence of potential synergistic effects between iron and other metals, particularly aluminum, in the *in vitro* aggregation of $A\beta_{42}$ [34]. Although $A\beta$ aggregates are a hallmark of AD, the role of $A\beta$ is contentious, with evidence both for and against its role in pathogenesis [19, 51].

Studies employing superconducting quantum interference device (SQUID) magnetometry and synchrotron X-ray analysis have enabled us to identify several iron compounds in samples of AD tissue [9,24]. These studies give? a preliminary indication that, in addition to ferritin/ferrihydrite, mixed valence state iron oxides (primarily magnetite – Fe_3O_4 – an iron oxide containing alternating lattices of ferric and ferrous iron) are also present in unusually high concentrations. This observation is particularly significant in that magnetite provides a source of ferrous iron (ferritin normally contains only ferric iron), that can promote the production of free radicals via the Fenton reaction [53].

The association of redox-active iron with AD senile plaques has been indicated using a modified histochemical stain [54], and quantification of iron in senile plaque cores, corona, and surrounding neuropil has been undertaken using micro particle-induced X-ray emission (microPIXE) to analyze fixed immunostained AD tissue sections. Here, elemental concentrations were found to be significantly higher in the plaque cores and corona than in the neuropil [38]. Recent transmission electron microscopy (TEM) analysis of AD plaque-rich tissue sections has indicated the presence of ferritin in the coronal plaque structure, among the bundles of the $A\beta$ fibers, and it was noted that the only electron-dense clusters evident in unstained sections were ferritin cores. In this same study, which used a nano-resolution secondary ion mass spectrometry (nanoSIMS) technique, iron was demonstrated in the periphery of senile plaques, but not in the plaque cores [47] – these may have been too dense to probe with the same efficiency as the surrounding tissue. In addition to studies of plaque cores in tissue sections, metal concentrations have been determined in isolated AD cores by inductively coupled plasma mass spectrometry (ICP-MS), where iron (followed in decreasing concentration by aluminum and zinc) was reported in the cores at concentrations of 2–20 mg/L [2].

Amyloid plaques have been studied by a host of techniques since their original observation by Blocq and Marinesco in 1892 [3]. The complete plaques are typically 5–20 μm in overall cross section. Plaques can take various forms ranging from neuritic diffuse structures, to classical plaques with an amyloid core, and more compact plaques with dense cores. The protein composition and conformation of extracted AD plaque core material has been investigated in detail using Ramen spectroscopy [15], demonstrating the dominance of the $A\beta_{42}$ peptide, but it has not proved straightforward to determine the structural properties of the dense core region. Original studies relied on time-consuming reconstructions of serial physical stained sections [31, 32,35,40,56,57]. Kato's confocal microscopy study of a series of Congo-red stained sections, cut at 0.4 μm thickness, revealed a coral-like structure in the computer reconstruction [31]. Rickert [49] employed reflection contrast microscopy to obtain optical sections through silver-stained amyloid plaques, performing three-dimensional reconstructions from the 1.5 μm virtual slices, but this study did not provide sufficient resolution to examine the internal structure of the cores.

Here, we have used electron tomography to obtain high-resolution reconstructions of amyloid plaque core material extracted from human AD brain tissue. This approach forgoes the need for staining or physical sectioning of the cores. In combination with energy dispersive X-ray (EDX) spectroscopy, electron energy-loss spectroscopy (EELS), high-resolution transmission electron microscopy (HR-TEM) and electron diffraction, it has allowed us to investigate the nature of iron-rich inclusions in isolated fragments of these amyloid plaque cores.

MATERIALS AND METHODS

To map and identify iron compounds in isolated AD plaque core material, peptide cores and core fragments were purified from frozen cortical brain tissue as previously described [14], sourcing tissue from two pathologically confirmed cases of AD, aged 76 and 81 years. Briefly, following homogenization in 2% sodium dodecyl sulphate (SDS), the sample was filtered through a 35 μm mesh and the plaque cores preliminarily separated within a sucrose gradient. The interface layers were collected, washed extensively with phosphate buffered saline (PBS) containing 0.1% SDS, and the particles separated by cell sorting, using both size and side-scatter parameters. The fraction containing the cores was suspended in PBS. The purity was checked at each stage by drying 5 μl samples on a glass microscope slide, staining with Congo red and counting the number of unstained particles and plaque cores which display birefringence when viewed under polarized light. Following cell sorting, the plaque cores, generally 5–10 μm in diameter, comprised $>$90% of all particles. However, many smaller core fragments were present in the sample. All solutions were made using MilliQ filtered water. A sample of cores extracted from these cases was also analyzed by Raman spectroscopy to confirm their protein composition and conformation [15].

Plaque core material, prepared as outlined above and suspended in PBS buffer, was pipetted onto Formvar film supported on 200-mesh copper grids (Agar Scientific Ltd., Essex, UK) and air-dried in a clean environment. Electron beam imaging was performed immediately afterwards.

Electron microscopy was carried out at 200 kV using a Tecnai F20-ST field emission gun TEM and at 300 kV using a Philips CM300-ST field emission gun TEM. Compositional information was obtained using both EDX spectroscopy and EELS [17]. Grids were initially scanned for electron-dense regions corresponding to core fragments (typically a few microns across), and EDX spectra were obtained to identify those exhibiting strong iron peaks. Iron rich fragments were imaged further using techniques including tomography (to create a virtual 3D reconstruction of the core), and diffraction (to determine crystalline structures associated with the plaque cores). Three-dimensional reconstructions of the local shapes, orientations and positions of regions of interest were obtained using high-angle annular dark-field (HAADF) electron tomography. Ultra-high-tilt series of HAADF images were acquired at 2° intervals over a tilt range of -70° to $+78^\circ$. The acquisition time for each image was 40 s. Since HAADF images are affected by diffraction contrast less strongly than bright-field images, they are better suited to tomographic reconstruction of crystalline specimens [41]. Digital processing of the images and visualization of the resulting tomographic reconstructions was carried out using FEI Xplore3D and Amira software. For off-axis electron holography [16], a technique that can be used to image magnetic fields in materials with sub-5-nm spatial resolution, a Lorentz mini-lens was used as the primary imaging lens, with the conventional electron microscope objective lens switched off. Reference holograms were acquired from vacuum immediately after each hologram of the specimen, and used to remove geometrical distortions associated with the imaging and recording system.

RESULTS

The plaque core materials, dispersed on the Formvar film, were initially located as electron-dense regions by TEM. Some core pieces had a roughly toroidal form, whilst others were smaller solid pieces. Core materials of various sizes and shapes were probed with EDX analysis to determine their elemental compositions. The majority of the pieces ($\sim$70%) had detectable levels of iron (Fe), although the measurements varied from strong peaks (as in Fig. 1) to trace levels in the EDX spectrum. Approximately half of the pieces studied also contained detectable levels of aluminum (Al). The same sites were examined using electron diffraction to look for evidence of crystallinity, and the strongest single crystal signals came from fragments that were rich in both Al and silicon (Si). Several core fragments exhibiting high concentrations of Fe and oxygen (O) (e.g., Fig. 1) were subjected to further analysis using techniques that include EELS.

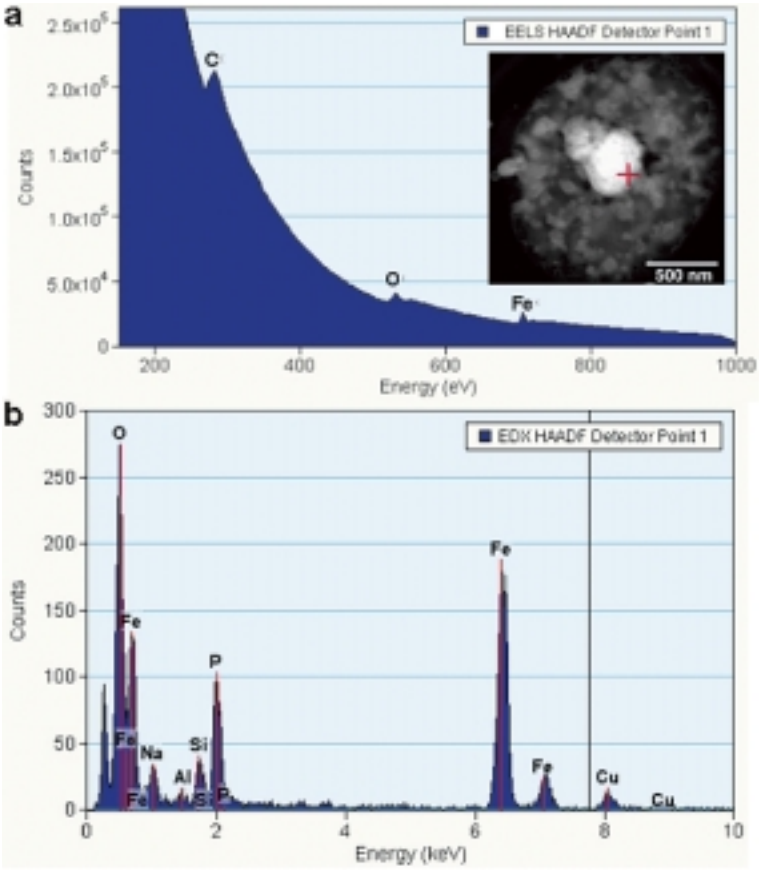

Fig. 1. Determination of the elements present in a core fragment. Data obtained in the Tecnai F20 TEM. (a) EELS spectrum and inset HAADF image showing the region analyzed using EELS and EDX spectroscopy. (b) EDX spectrum acquired from the position marked with a cross in Fig. 1a.

For the example shown in Fig. 1, we note that in addition to major concentrations of Fe, O, and carbon (C), moderate levels of phosphorus (P), sodium (Na), and Si were detected. Minor signals from Al, magnesium (Mg), calcium (Ca) and potassium (K) were also recorded. Sulfur is notably absent, which is consistent with Raman spectroscopy data from isolated cores, in which the only anticipated source is the sulfur-bearing peptide, methionine, in concentrations that are too low to be detected using EDX spectroscopy [15]. The presence of Cu has been demonstrated in previous studies of AD plaque cores [15,38], but the possibility that some or all the Cu signal in Fig. 1 originates from scattering from the Cu mesh of the TEM grid cannot be discounted. The spectra shown in Fig. 1 are typical of those observed for many of the core fragments, although the relative proportions of the elements varied significantly, and some exhibited higher levels of Al than Fe.

In order to investigate the dense regions of the AD plaque cores, we used high-angle annular dark-field electron tomography to produce high-resolution three-dimensional reconstructions of two of the iron-rich isolated AD plaque core fragments, without the need for staining or physical cross-sectioning. The images in Fig. 2 show one such reconstruction of the fragment from Fig. 1, within which electron-dense nanoscale particulates were observed. Tomographic imaging clearly demonstrates that the electron-dense particles are found to be distributed within the plaque material rather than aggregated on the surface (Fig. 2). The boundary containing the dense particles is outlined in orange in Fig. 2a, and the corresponding volume is enclosed in orange in Fig. 2b.

Having confirmed the presence of Fe and O in core fragments containing dense nanoscale particle inclusions, the fragments were then analyzed to determine the crystalline states of the particles, and in particular to establish whether they corresponded to known iron oxides. Both the electron diffraction patterns and the high-resolution lattice images acquired from the individu-

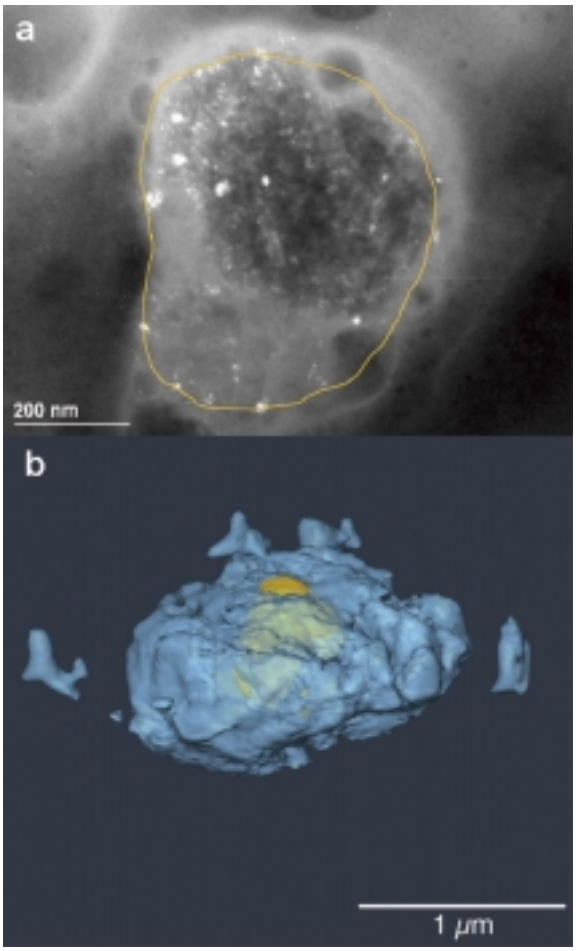

Fig. 2. (a) Representative dark-field image of the plaque core material shown in Fig. 1, obtained in a Philips CM300 TEM by selecting parts of the magnetite/maghemite ring pattern. The magnetite/maghemite particles appear bright. (b) Tomographic reconstruction of plaque material, determined from HAADF images obtained in the Tecnai F20 TEM, with the approximate outlined region from (a) – indicating the location of magnetite/maghemite particles – highlighted in orange.

al particles and polycrystalline aggregates were consistent with those expected for magnetite/maghemite (Fig. 3). The measured lattice parameters were consistent only with magnetite/maghemite (Table 1) and not with any other known crystalline biological iron compounds such as ferrihydrite (the iron oxyhydroxide core of ferritin), or with goethite-like iron oxides associated with hemosiderin [48], or wüstite [45]. This observation indicates that biogenic magnetite/maghemite is not only present, but is the dominant form of iron in the electron-dense particles examined within the iron-rich core fragment.

Off-axis electron holography was performed in order

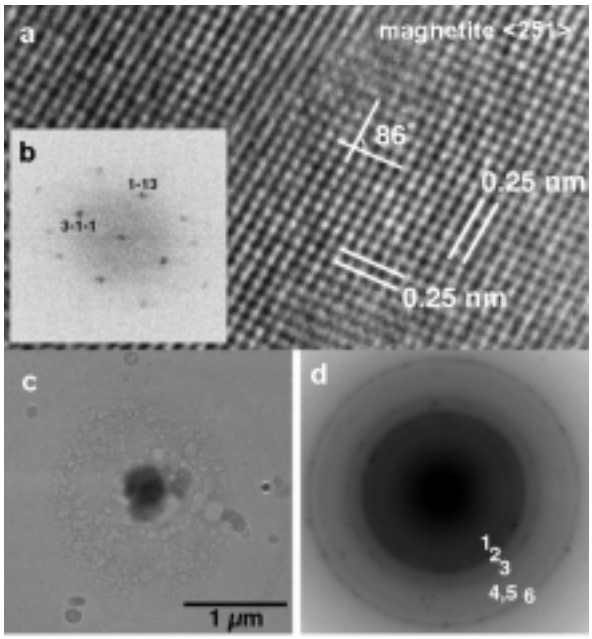

Fig. 3. Images and electron diffraction patterns acquired from the core fragment examined in the Philips CM30. (a) High-resolution electron microscopy (HR-TEM) image of one of the electron-dense regions within the plaque core. The lattice fringe spacings and angles are consistent with those expected for <251> magnetite or maghemite. (b) Inset power spectrum (Fourier transform) of the HR-TEM image shown in Fig. 3a. (c) Bright-field image and (d) polycrystalline electron diffraction rings recorded from the electron-dense region shown in Fig. 3a. The measured lattice spacings are given in Table 1.

to image the magnetic flux lines arising from the particles within the plaque core shown in Fig. 2. Analysis of these regions did not reveal a measurable magnetic signal, indicating that the particles do not preserve a detectable stable, remanent magnetization. This finding is consistent with a superparamagnetic response (Fig. 4). For biogenic magnetite at room temperature, the critical size for magnetization blocking (below which a particle of magnetite/maghemite would be superparamagnetic) is on the order of 20–30 nm (although this value is dependent on particle shape and spacing). The magnetite/maghemite particles observed by dark-field TEM in this same core fragment (Fig. 2a) appear to have irregular shapes, and when measured ($n = 75$) the majority were found to be in the 2 to 7 nm size range, with a mean diameter M of 6.9 nm (Fig. 5). A few larger particles (8–40 nm) were also observed, although these may have been aggregates of smaller particles. The larger particles may be responsible for the low coercivity remanent magnetization recently observed in high sensitivity SQUID measurements of AD tissue [24].

Table 1
Comparison of the measured lattice spacings ('core sample') with those of known Fe oxides, hydroxides and oxyhydroxides

Core sample		0.299		0.253		0.210			0.163		0.148	
Magnetite Fe_3O_4	0.485 (11)	0.297 (30)		0.253 (100)		0.210 (21)			0.161 (28)		0.148 (37)	
Maghemite γFe_2O_3		0.295 (35)		0.252 (100)		0.209 (16)			0.161 (24)		0.148 (34)	
Ferrihydrite1 $Fe_2O_3nH_2O$				0.25	0.22–0.23	0.2		0.17		0.15		
Ferrihydrite2 $Fe_2O_3nH_2O$				0.25 (100)	0.221 (80)	0.196 (80)		0.172 (50)		0.151 (70)	0.148 (80)	
Goethite FeO(OH)	0.418 (100)		0.269 (35)	0.245 (50)	0.219 (18)	0.209 (1)						
Hematite Fe_2O_3	0.368 (31)		0.27 (100)	0.252 (70)	0.22 (19)		0.184 (34)	0.17 (41)				
Wüstite FeO				0.25 (68)	0.216 (100)					0.15 (47)		0.13 (17)
Ferroxyhyte FeO(OH)	0.461 (20)			0.255 (100)	0.226 (100)			0.16 (100)			0.147 (100)	
Lepidocrocite FeO(OH)	0.626 (100)	0.297 (10)		0.247 (80)	0.236 (20)	0.194 (70)		0.173 (40)		0.152 (40)		0.329 (90)
Akaganeite FeO(OH)	0.333 (100)			0.255 (55)	0.230 (35)	0.195 (20)			0.164 (35)			0.746 (40)

Lattice parameters are given in nm, and the numbers in brackets indicate relative intensities.

Despite the long imaging times, the samples were not appreciably damaged in the electron beam. HAADF scanning transmission electron microscopy (STEM) tomographic imaging has been shown to cause less damage to organic materials than broad beam techniques such as conventional bright-field imaging [20, 44]. However, it was not possible to apply the full range of analytical techniques to all of the iron-rich core fragments that were identified. Although the dense plaque core material proved to be very stable in the electron beam, the Formvar film was not always sufficiently robust for diffraction to be completed after electron tomography had been carried out. Care was taken to ensure that Figs 1–5 corresponded to a specific core fragment in order to provide a complete interpretation. Complete tomographic reconstruction of a second iron-rich plaque core found in another grid region (Fig. 6) also revealed electron-dense particles embedded in plaque core material, as seen in the other documented example. The second tomographic example shown in Fig. 6 (with an HAADF image presented alongside a pair of reconstructed cross-sectional virtual 'slices' and a complete 3D rendering of the fragment), is typical of the toroidal fragments observed on the grid.

DISCUSSION

Under normal conditions, iron is stored in a primarily ferrihydrite-like structure ($5Fe_2O_3\ 9H_2O$), containing only ferric (Fe^{3+}) iron within the core of the hollow, spherical iron-storage protein ferritin. Recent evidence indicates that polyphase cores may be present in both normal physiological and pathological brain ferritin [13,29,30,46]. In particular, HR-TEM and electron diffraction have been used to demonstrate that a cubic iron oxide distinct from the dominant ferrihydrite-like crystal structure observed in normal human brain ferritin, and consistent with magnetite/maghemite, is a major phase in AD ferritin cores [29,46]. Likewise, EELS has been used to show the presence of both Fe^{2+} and Fe^{3+} in individual ferritin particles present in preparations of isolated PSP-tau and AD-paired helical filaments [45].

The diameter of a ferritin protein's internal cavity is 8 nm, which restricts the size of the crystals that precipitated within it. If the biogenic magnetite/maghemite observed in this study is forming from a ferritin/ferrihydrite precursor, then one potential mechanism for its formation is a disruption of the ferritin protein's ability to oxidize ferrous iron as it is transported into the internal cavity [8,10,45]. From the size distribution of the magnetite/maghemite particles observed in the plaque core material (Fig. 5), it is evident that the majority of the particles are below 8 nm in diameter, but that a significant proportion of the total magnetite volume is associated with particles or particle aggregates that are greater than 8 nm in diameter. If one makes the assumption that

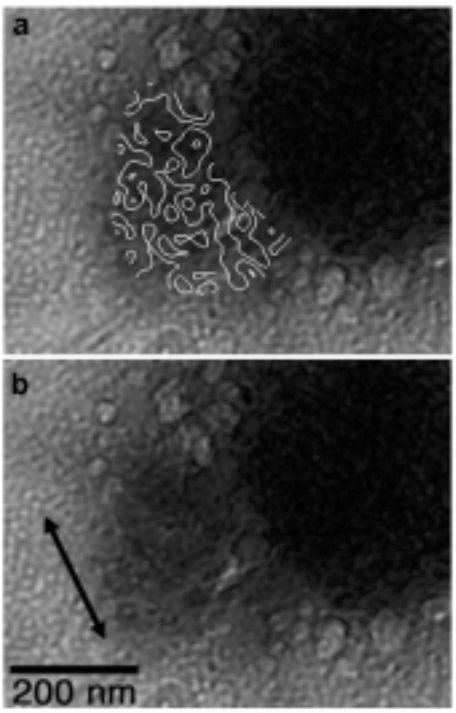

Fig. 4. Electron holographic magnetic induction map acquired from the core fragment in zero applied magnetic field, in the Philips CM300. The phase contours shown in (a) are from the same region that was used to acquire the HR-TEM image shown in Fig. 3, and should reveal a magnetic signal if one were present. The observed contours are due to statistical noise. Their spacing is 0.049 radians. In (b) the direction of the magnetic field applied to the sample before recording the holograms is shown.

the magnetite/maghemite particles originated from ferritin/ferrihydrite precursors, then the larger particles observed in the plaque core material may be aggregates or clusters of small crystals that originally formed within the ferritin shell, or particles that may have grown beyond this dimension following the breakdown of the protein shell.

Using EDX and electron diffraction, it was not possible to distinguish between magnetite and its oxidation product, maghemite – which has very similar crystallography, composition, and magnetic properties. In addition, due to the thickness of the samples examined in the present study, the EELS spectra precluded determination of the valence state of the iron, which would have allowed differentiation between magnetite and maghemite. In supporting studies, our analyses of intact AD tissue sections using X-ray absorption spectroscopy (XAS) indicate the presence of highly localized magnetite accumulations, and that the majority of the iron anomalies observed are due to either magnetite or abnormal accumulations of ferrihydrite [9]. Oxidation of magnetite to maghemite may occur post mortem, but in the event that magnetite is converted to maghemite *in vivo*, the oxidation of Fe^{2+} may contribute to the generation of free radicals via Fenton chemistry. This mechanism is likely to be even more important for processes that take place inside the protein shell due to the role of H_2O_2 at the L- and H-chain ferroxidase sites [60]. In addition, the magnetic fields that are generated by larger crystals of both magnetite and maghemite can influence biochemical reaction rates and produce free radicals via triplet state stabilization [52,55].

The presence of magnetite in human brain tissue has been demonstrated in numerous studies [4,9,24,25,36] including senile-plaque-rich tissues from AD autopsy cases [9,24]. The formation of nanoscale magnetite particles has been studied widely under *in vitro* conditions, but the mechanisms for its formation *in vivo* are not understood. Magnetite contains both ferrous and ferric iron. Under normal conditions, the concentration of ferrous iron is regulated by the uptake and storage in ferritin of iron in its less reactive ferric state. Khan et al. [34] recently demonstrated that, in a buffered solution at pH 7.4, ferric iron is reduced to the ferrous state in the presence of aggregating $A\beta_{42}$ peptide. It is worth noting that detectable aluminum signals were obtained from approximately half of the plaque core fragments in the present study, and that Khan et al. demonstrated that the addition of a pathophysiologically significant concentration of Al^{3+} potentiated the redox cycle in favor of Fe^{2+}. These striking findings indicate a mechanism by which interactions between $A\beta_{42}$ and iron may produce elevated concentrations of toxic ferrous iron at sites of amyloid pathology, and provides a potential route by which magnetite may form *in vivo*.

Although it is not yet clear whether the presence of biogenic magnetite/maghemite within the plaque core contributes to AD pathogenesis, its presence may be of diagnostic utility. Iron deposits, associated with amyloid pathology and microbleeds, are increasingly noted in magnetic resonance imaging (MRI) studies [18,28,32,37,42]. These are typically attributed to hemosiderin [48] from microbleeds in the vicinity of amyloid pathology, and it would be of diagnostic and potentially therapeutic value to confirm the precise nature of these iron-rich inclusions. Synthetic magnetite nanoparticles (also called superparamagnetic iron oxides, or SPIOs) are used routinely as contrast agents for MRI. The presence of *biogenic* magnetite/maghemite associated with AD tissue may be useful for the development of MRI-based early detection techniques based

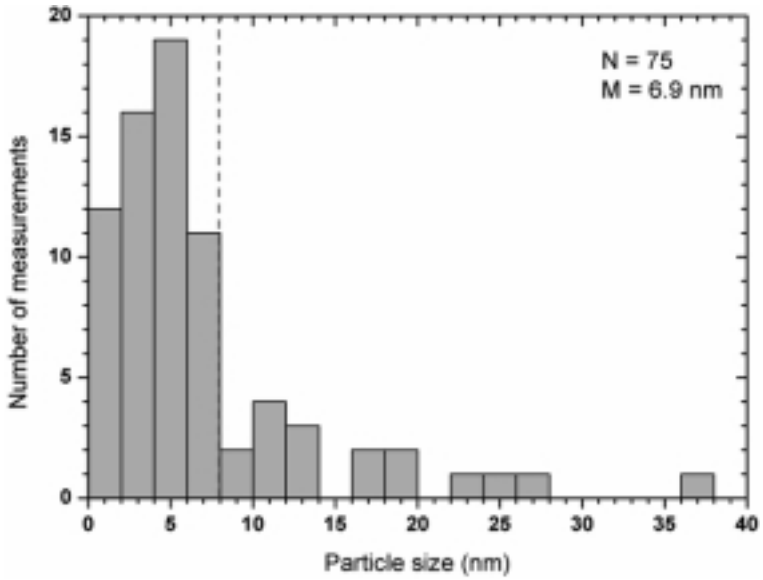

Fig. 5. Measured size distribution of 75 electron-dense particles from within the core, determined from multiple dark-field images obtained on a Philips CM300 TEM (see for example Fig. 2a). The mean value M is characteristic of the size of the ferrihydrite core of the iron storage protein ferritin, although several particles observed were larger than the maximum possible core size of 8 nm. The dashed line represents the maximum core size that would fit within the ferritin protein.

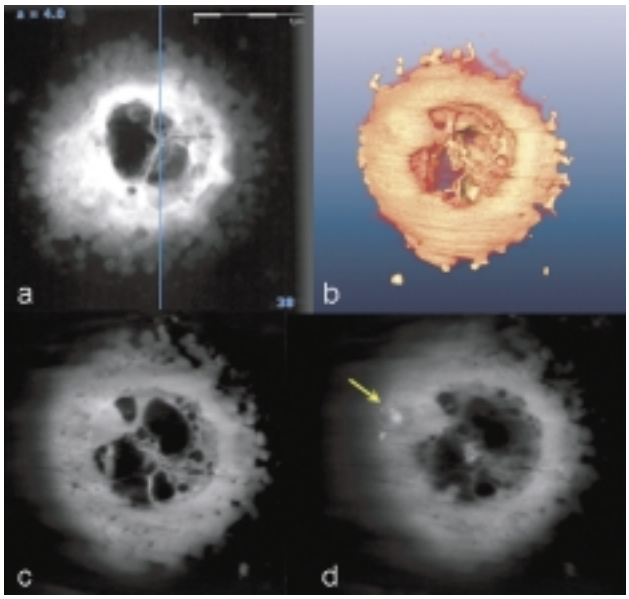

Fig. 6. Example of a three-dimensional reconstruction of one of the amyloid plaque core fragments, determined using high-angle annular dark-field electron tomography: (a) image 38 from the original sequence of 75 HAADF images, scale bar is 1 μm; (b) reconstruction of fragment from the full sequence; (c) and (d) cross-sections that allow the internal structure of the fragment to be visualized. In (d), an example of higher density nanoscale regions embedded within the structure is arrowed.

on the formation of magnetic iron compounds that will act as "natural" contrast agents. In addition, knowledge of the specific iron compounds that are associated with AD pathology may guide the development of potential therapeutic chelating compounds.

Studies of gel phantoms indicate that levels of biogenic magnetite in the range of a few micrograms of magnetite per gram of tissue are detectable with clini-

cal 1.5T scanners [43]. Isothermal remanent magnetization (IRM) analysis at 0°C performed by Kirschvink et al. [36] shows magnetite/maghemite concentrations in the ng/g range. However, magnetization versus field measurements, which will also include superparamagnetic magnetite, indicate *total* magnetite concentrations in AD samples in the μg/g region [24]. Although magnetometry analysis of larger samples indicates concentrations around or below detectable limits, synchrotron studies of tissue sections clearly show that it is inhomogeneously distributed, with highly localized concentrations that should be detectable within individual MRI voxels [9]. In addition, with the proliferation of new 3T scanners, local, high concentrations of biogenic magnetite/maghemite on the order of that observed in these studies should be more easily detectable. This observation is particularly relevant as local ferritin (ferrihydrite) levels are also raised in association with AD [9] and investigations are already underway to exploit this capability for MRI-based early detection of AD [1,27, 28].

If the formation of biogenic magnetite occurs due to processes that affect ferritin in the early stages of AD, it may be possible to detect its presence before clinical symptoms become apparent – perhaps even before significant aggregation of Aβ plaque material – by altering MRI pulse sequences. This possibility is particularly important as new drugs that are in development for AD are aimed primarily at slowing or halting the progression of the disease rather than at reversing its effects. Therefore, the early administration of these drugs is crucial.

In a broader context, the importance of understanding potential connections between iron and neurodegeneration in other diseases should not be overlooked. Recent research has led to the development of iron chelators as a potential therapeutic agent for neurodegenerative diseases [58]. As iron plays an important role in dopamine synthesis, the wholesale removal of readily-available iron via chelation could potentially exacerbate the problem. It is therefore of profound importance to understand which (and whether) specific iron compounds are related to disease and which are required for normal brain function.

Although the present study highlights important gaps in our understanding of the *in vivo* connection between iron metabolism and amyloid toxicity, it is clear that the expected iron compounds, ferrihydrite and goethite-like iron oxides associated with hemosiderin, are not dominant within the iron-rich plaque core material examined here. Our results, along with *in vitro* studies showing that iron influences Aβ aggregation and that Aβ can reduce iron under physiological conditions [34], provide strong evidence that iron is involved in AD pathogenesis – either directly, due to its role in free radical production, or indirectly as a product of a breakdown in brain ferritin function.

ACKNOWLEDGMENTS

This work is supported by NIH Grants R01 AG02030-01 and 1R21NS060304-01, the Alzheimer's Society (UK), and the Dunhill Medical Trust (UK). JFC is supported by EPSRC Life Sciences Interface grant EP/D066654/1 and an RCUK Fellowship. JD is supported by a Royal Society Wolfson Merit Award. We thank several anonymous reviewers for their valuable contributions towards improving this manuscript. Dr. Smith is, of has in the past been, a paid consultant for, owns equity or stock options in and/or receives grant funding from Neurotez, Neuropharm, Edenland, Panacea Pharmaceuticals, and Voyager Pharmaceuticals. Dr. Perry is a paid consultant for and/or owns equity or stock options in Takeda Pharmaceuticals, Voyager Pharmaceuticals and Panancea Pharmaceuticals.

References

[1] G. Bartzokis, T.A. Tishler, P.H. Lua, P. Villablanca, L.L. Altshuler, M. Carter, D. Huanga, N. Edwards and J. Mintz, Brain ferritin may influence age- and gender-related risks of neurodegeneration, *Neurobiol Aging* **28** (2007), 414–423.

[2] D. Beauchemin and R. Kisilevsky, A method based on ICP-MS for the analysis of Alzheimer's amyloid plaques, *Anal Chem* **70** (1998), 1026–1029.

[3] P. Blocq and G. Marinesco, Sur les lesions et la pathogenie de l'epilepsie die essentielle, *Sem Med* **12** (1892), 445–446.

[4] F. Brem, A.M. Hirt, M. Winklhofer, K. Frei, Y. Yonekawa, H.G. Wieser and J. Dobson, Magnetic iron compounds in the human brain: a comparison of tumour and hippocampal tissue, *J R Soc Interface* **3** (2006), 833–841.

[5] R.J. Castellani, S.L. Siedlak, G. Perry and M.A. Smith, Sequestration of iron by Lewy bodies in Parkinson's disease, *Acta Neuropathol* **100** (2000), 111–114.

[6] R.J. Castellani, H.G. Lee, X. Zhu, A. Nunomura, G. Perry and M.A. Smith, Neuropathology of Alzheimer disease: pathognomonic but not pathogenic, *Acta Neuropathol* (*Berl*) **111** (2006), 503–509.

[7] R.J. Castellani, P.I. Moreira, G. Liu, J. Dobson, G. Perry, M.A. Smith and X. Zhu, Iron: the redox-active center of oxidative stress in Alzheimer disease, *Neurochem Res* **32** (2007), 1640–1645.

[8] N.D. Chasteen and P.M. Harrison, Mineralization in ferritin: an efficient means of iron storage, *J Struct Biol* **126** (1999), 182–194.

[9] J.F. Collingwood, A. Mikhaylova, M. Davidson, C. Batich, W.J. Streit, J. Terry and J. Dobson, In situ characterization and mapping of iron compounds in Alzheimer's tissue, *J Alzheimers Dis* **7** (2005), 267–272.
[10] J.F. Collingwood and J. Dobson, Mapping and characterization of iron compounds in Alzheimer's tissue, *J Alzheimers Dis* **10** (2006), 215–222.
[11] J.F. Collingwood and J. Dobson, Nanoscale iron compounds related to neurodegenerative disorders, in: *Biomedical Nanostructures*, K.E. Gonsalves, C.R. Halberstadt, C.T. Laurencin and L.S. Nair, eds, John Wiley & Sons, New Jersey, 2007, pp. 461–490.
[12] J.R. Connor, B.S. Snyder, P. Arosio, D.A. Loeffler and P. LeWitt, A quantitative analysis of isoferritins in selected regions of aged, parkinsonian, and Alzheimer's diseased brains, *J Neurochem* **65** (1995), 717–724.
[13] J.M. Cowley, D.E. Janney, R.C. Gerkin and P.R. Buseck, The structure of ferritin cores determined by electron nanodiffraction, *J Struct Biol* **13** (2000), 210–216.
[14] D.A. DeWitt, G. Perry, M. Cohen, C. Doller and J. Silver, Astrocytes regulate microglial phagocytosis of senile plaque cores of Alzheimer's disease, *Exp Neurology* **149** (1998), 329–340.
[15] J. Dong, C.S. Atwood, V.E. Anderson, S.L. Siedlak, M.A. Smith, G. Perry and P.R. Carey, Metal binding and oxidation of amyloid-β within isolated senile plaque cores: Raman microscopic evidence, *Biochemistry* **42** (2003), 2768–2773.
[16] R.E. Dunin-Borkowski, M.R. McCartney and D.J. Smith, in: *Encyclopaedia of Nanoscience and Nanotechnology*, (Vol. 3), H.S. Nalwa, ed., American Scientific Publishers, 2004, pp. 41–100.
[17] R.F. Egerton, *Electron Energy-loss Spectroscopy in the Electron Microscope*, Plenum Press, New York, 1986.
[18] C. Faber, B. Zahneisen, F. Tippmann, A. Schroeder and F. Fahrenholz, Gradient-echo and CRAZED imaging for minute detection of Alzheimer plaques in an APPV717I x ADAM10-dn mouse model, *Magn Reson Med* **57** (2007), 696–703.
[19] J.C. Fiala, Mechanisms of amyloid plaque pathogenesis, *Acta Neuropathologica* **114** (2007), 551–571.
[20] M.H. Gass, K.K. Koziol, A.H. Windle and P.A. Midgley, Four-dimensional spectral tomography of carbonaceous nanocomposites, *Nano Letters* **6** (2006), 376–379.
[21] B.B. Gelman, Iron in CNS disease, *J Neuropathol Exp Neurol* **54** (1995), 477–486.
[22] L. Goodman, Alzheimer's disease – a clinicopathologic analysis of 23 cases with a theory on pathogenesis, *J Nerv Ment Dis* **118** (1953), 97–130.
[23] B. Hallgren and P. Sourander, The non-haemin iron in the cerebral cortex in Alzheimer's disease, *J Neurochem* **3** (1958), 41–51.
[24] D. Hautot, Q.A. Pankhurst, N. Khan and J. Dobson, Preliminary evaluation of nanoscale biogenic magnetite and Alzheimer's disease, *Proc Royal Soc Lon B: Biol Lett* **270** (2003), S62–S64.
[25] D. Hautot, Q.A. Pankhurst, C.M. Morris, A. Curtis, J. Burn and J. Dobson, Preliminary observation of elevated levels of nanocrystalline iron in the basal ganglia of neuroferritinopathy patients, *Biochim Biophys Acta* **1772** (2007), 21–25.
[26] E. House, J. Collingwood, A. Khan, O. Korchazkina, G. Berthon and C. Exley, Aluminium, iron, zinc and copper influence the *in vitro* formation of amyloid fibrils of Aβ42 in a manner which may have consequences for metal chelation therapy in Alzheimer's disease, *J Alzheimers Dis* **6** (2004), 291–301.
[27] M.J. House, T.G. St. Pierre, K.V. Kowdley, T. Montine, J. Connor, J. Beard, J. Berger, N. Siddaiah, E. Shankland and L.W. Jin, Correlation of proton transverse relaxation rates (R_2) with iron concentrations in postmortem brain tissue from Alzheimer's disease patients, *Magn Reson Med* **57** (2007), 172–180.
[28] C.R. Jack, T.M. Wengenack, D.A. Reyes, M. Garwood, G.L. Curran, B.J. Borowski, J. Lin, G.M. Preboske, S.S. Holasek, G. Adriany and J.F. Poduslo, *In vivo* magnetic resonance microimaging of individual amyloid plaques in Alzheimer's transgenic mice, *J Neurosci* **25** (2005), 10041–10048.
[29] D.E. Janney, J.M. Cowley and P.R. Buseck, Structure of synthetic 2-line ferrihydrite by electron nanodiffraction, *Amer Mineral* **85** (2000), 1180–1187.
[30] D.E. Janney, J.M. Cowley and P.R. Buseck, Transmission electron microscopy of synthetic 2- and 6-line ferrihydrite, *Clays Clay Miner* **48** (2000), 111–119.
[31] S. Kato, T. Gondo, Y. Hoshii, M. Takahashi, M. Yamada and T. Ishihara, Confocal observation of senile plaques in Alzheimer's disease: Senile plaque morphology and relationship between senile plaques and astrocytes, *Pathol Int* **48** (1998), 332–340.
[32] M. Kawai, P. Cras and G. Perry, Serial reconstruction of amyloid plaques: Relationship to microvessels and size distribution, *Brain Res* **592** (1992), 278–282.
[33] Y. Ke and Z. Qian, Iron misregulation in the brain: a primary cause of neurodegenerative disorders, *Lancet Neurol* **2** (2003), 246–253.
[34] A. Khan, J. Dobson and C. Exley, Redox cycling of iron by Aβ42, *Free Radic Biol Med* **40** (2006), 557–569.
[35] T. Kimura, T. Hisano, H. Yoshida, K. Ueda and T. Miyakawa, Re-evaluation of classic senile plaques by three-dimensional analysis, *J Neurol* **241** (1994), 624–627.
[36] J.L. Kirschvink, A. Kobayashi-Kirschvink and B.J. Woodford, Magnetite biomineralization in the human brain, *Proc Natl Acad Sci USA* **89** (1992), 7683–7687.
[37] S.P. Lee, M.F. Falangola, R.A. Nixon, K. Duff and J.A. Helpern, Visualization of beta-Amyloid plaques in a transgenic mouse model of Alzheimer's disease using MR microscopy without contrast reagents, *Magn Reson Med* **52** (2004), 538–544.
[38] M.A. Lovell, J.D. Robertson, W.J. Teesdale, J.L. Campbell and W.R. Markesbery, Copper, iron and zinc in Alzheimer's disease senile plaques, *J Neurol Sci* **158** (1998), 47–52.
[39] M.W. Marlatt, K.M. Webber, P.I. Moreira, H. Lee, G. Casadesus, K. Honda, X. Zhu, G. Perry and M.A. Smith, Therapeutic opportunities in Alzheimer disease: one for all or all for one? *Curr Med Chem* **12** (2005), 1137–1147.
[40] E. Masliah, M. Mallory, T. Deerinck, R. DeTeresa, S. Lamont, A. Miller, R.D. Terry, B. Carragher and M. Ellisman, Re-evaluation of the structural organization of neuritic plaques in Alzheimer's disease, *J Neuropath Exp Neurol* **52** (1993), 619–632.
[41] P.A. Midgley, M. Weyland, J.M. Thomas and B.F.G. Johnson, Z-Contrast tomography: a technique in three-dimensional nanostructural analysis based on Rutherford scattering, *Chem Comm* **10** (2001), 907–908.
[42] Y. Nakata-Kudo, T. Mizuno, K. Yamada, K. Shiga, K. Yoshikawa, S. Mori, T. Nishimura, K. Nakajima and M. Nakagawa, Microbleeds in Alzheimer disease are more related to cerebral amyloid angiopathy than cerebrovascular disease, *Dement Geriatr Cogn Disord* **22** (2006), 8–14.
[43] H. Pardoe, W. Chua-anusorn, T.G. St. Pierre and J. Dobson, Detection limits for ferromagnetic particle concentrations us-

ing magnetic resonance imaging-based proton transverse relaxation rate measurements, *Phys Med Biol* **48** (2003), 89–95.
[44] A.E. Porter, M. Gass, K. Muller, J.N. Skepper, P.A. Midgley and M. Welland, Direct imaging of single-walled carbon nanotubes in cells, *Nat Nanotechnol* **2** (2007), 713–717.
[45] C. Quintana, M. Lancin, C. Marhic, M. P'erez, J.Avila and J.L. Carrascosa, Preliminary high-resolution TEM and electron energy-loss spectroscopy studies of ferritin cores extracted from brain in patients with neurodegenerative PSP and Alzheimer diseases, *Cell Molec Biol* **46** (2000), 807–820.
[46] C. Quintana, J.M. Cowley and C. Marhic, Electron diffraction and high-resolution electron microscopy studies of the structure and composition of physiological and pathological ferritin, *J Struct Biol* **147** (2004), 166–178.
[47] C. Quintana, S. Bellefqih, J.Y. Laval, J.L. Guerquin-Kern, T.D. Wu, J. Avila, I. Ferrer, R. Arranz and C. Patiño, Study of the localization of iron, ferritin, and hemosiderin in Alzheimer's disease hippocampus by analytical microscopy at the subcellular level, *J Struc Biol* **153** (2006), 42–54.
[48] C. Quintana, About the Presence of Hemosiderin in the Hippocampus of Alzheimer Patients, *J Alzheimers Dis* **12** (2007), 157–160.
[49] C.H. Rickert, T.J. Fuller and F. Gullotta, Three-dimensional reconstruction of senile plaques in Alzheimer's disease, *J Microscopy* **186** (1997), 263–269.
[50] C.A. Rottkamp, A.K. Raina, X. Zhu, E. Gaier, A.I. Bush, C.S. Atwood, M. Chevion, G. Perry and M.A. Smith, Redox-active iron mediates amyloid-β toxicity, *Free Radic Biol Med* **30** (2001), 447–450.
[51] C.A. Rottkamp, C.S. Atwood, J.A. Joseph, A. Nunomura, G. Perry and M.A. Smith, The state versus amyloid-beta: the trial of the most wanted criminal in Alzheimer disease, *Peptides* **23** (2002), 1333–1341.
[52] J.C. Scaiano, S. Monahan and J. Renaud, Dramatic effects of magnetite particles on the dynamics of photogenerated free radicals, *Photochem Photobiol* **65** (1997), 759–762.
[53] D. Schubert and M. Chevion, The role of iron in beta amyloid toxicity, *Biochem Biophys Res Comm* **216** (1995), 702–707.
[54] M.A. Smith, P.L.R. Harris, L.M. Sayre and G. Perry, Iron accumulation in Alzheimer disease is a source of redox-generated free radicals, *Proc Natl Acad Sci USA* **94** (1997), 9866–9868.
[55] C.R. Timmel, U. Till, B. Brocklehurst, K.A. McLauchlan and P.J. Hore, Effects of weak magnetic fields on free radical recombination reactions, *Mol Phys* **95** (1998), 71–89.
[56] J. Wegiel and H.M. Wisniewski, The complex of microglial cells and amyloid star in three-dimensional reconstruction, *Acta Neuropathol* **81** (1990), 116–124.
[57] H.M. Wisniewski, A.W. Vorbrodt, J. Weigel, J. Morys and A.S. Lossinsky, Ultrastructure of the cells forming amyloid fibres in Alzheimer disease and scrapie, *Am J Med Gen Suppl* **7** (1990), 287–297.
[58] L. Zecca, M.B. Youdim, P. Riederer, J.R. Connor and R.R. Crichton, Iron, brain ageing and neurodegenerative disorders, *Nat Rev Neurosci* **5** (2004), 863–873.
[59] L. Zecca, M. Gallorini, V. Schünemann, A.X. Trautwein, M. Gerlach, P. Riederer, P. Vezzoni and D. Tampellini, Iron, neuromelanin and ferritin in substantia nigra of normal subjects at different ages. Consequences for iron storage and neurodegenerative disorders, *J Neurochem* **76** (2001), 1766–1773.
[60] G. Zhao, F. Bou-Abdallah, P. Arosio, S. Levi, C. Janus-Chandler and N.D. Chasteen, Multiple pathways for mineral core formation in mamallian apoferritin: The role of hydrogen peroxide, *Biochemistry* **42** (2003), 3142–3150.